1 September 2000

ELSEVIER

Chemical Physics Letters 327 (2000) 69–75

CHEMICAL PHYSICS LETTERS

www.elsevier.nl/locate/cplett

Enhanced saturation lithium composition in ball-milled single-walled carbon nanotubes

B. Gao [1], C. Bower, J.D. Lorentzen, L. Fleming, A. Kleinhammes, X.P. Tang, L.E. McNeil, Y. Wu, O. Zhou [*,1]

Department of Physics and Astronomy, University of North Carolina at Chapel Hill, Chapel Hill, NC 27599, USA

Received 9 May 2000; in final form 13 July 2000

Abstract

The effects of processing on the structure and morphology of single-walled carbon nanotubes (SWNT) and their electrochemical intercalation with lithium were investigated. Purified SWNTs were processed by impact ball-milling and were electrochemically intercalated with lithium. The reversible saturation Li composition increased from $Li_{1.7}C_6$ in purified SWNTs to $Li_{2.7}C_6$ after 10 min of milling. The irreversible capacity decreased from $Li_{3.2}C_6$ to $Li_{1.3}C_6$. Electron microscopy, Raman and X-ray diffraction measurements indicated that ball-milling induced disorder within the bundles and fractured the nanotubes. © 2000 Published by Elsevier Science B.V.

Intercalation compounds of carbon materials are of considerable interest and have been investigated in detail. Intercalation of C_{60} fullerene with alkali metals led to the discovery of superconductivity in metal fullerides with transition temperatures surpassed only by the high-T_c oxides [1]. Lithium intercalated graphite and carbonaceous materials are commercially used in Li-ion batteries [2] where the specific energy capacity is partially limited by the thermodynamic equilibrium saturation composition of LiC_6 (372 mAh/g) [3]. Because of their structure and chemical bonding, carbon nanotubes are interesting one-dimensional (1D) intercalation hosts. Compared to graphite and C_{60}, nanotubes can potentially have a higher saturation composition by accommodating guest species in the interstitial sites inside the nanotubes, between the graphene shells and between the nanotubes. They have been suggested as candidate high energy density anode materials for rechargeable Li-ion batteries.

Two types of carbon nanotubes can now be synthesized. The multi-walled carbon nanotubes (MWNT) are composed of concentric and closed graphene tubules [4]. Alkali metals can be intercalated into the inter-shell van der Waals spaces within the same MWNTs through defect sites to a saturation composition of MC_8 (M = K, Rb, Cs) [5,6]. The second type, the single-walled nanotubes (SWNT), forms bundles held together by van der Waals forces [7]. Vapor-phase transport reactions between alkali metals and as-grown SWNT mats yield a saturation composition of MC_8 (M = K, Rb, Cs) [8,9]. Raman experiments indicated that the alkali metals donated electrons to the SWNTs [10]. Due to disorder within

* Corresponding author. Fax: +1-919-962-0480; e-mail: zhou@physics.unc.edu

[1] Curriculum in Applied and Materials Sciences.

0009-2614/00/$ - see front matter © 2000 Published by Elsevier Science B.V.
PII: S0009-2614(00)00851-4

the bundle upon intercalation [11,12], the exact location of the alkali metals in the intercalated SWNTs is unknown.

Reversible electrochemical intercalation of SWNT bundles with Li has recently been demonstrated [12,13]. Purified SWNTs show a reversible saturation composition of $Li_{1.7}C_6$ [13], considerably higher than the LiC_6 ideal value for graphite and that reported for MWNTs [14]. In this Letter, we show that the reversible saturation Li composition of the SWNTs can be increased to as high as $Li_{2.7}C_6$ (1000 mAh/g) after ball-milling. The process induces disorder within the SWNT bundles and fractures the individual nanotubes.

The SWNT bundles used in this study were synthesized by the laser ablation method [7]. As-grown materials were purified by filtering the impurity phases through a micro-pore membrane while keeping the nanotubes in suspension for several hours using a high-power ultrasonic horn [15]. Transmission (TEM) and scanning (SEM) electron microscopy examinations indicated that the purified materials contain over 80% of SWNT bundles, 10–40 nm in bundle diameter and 1.3–1.6 nm in individual nanotube diameter. After vacuum annealing at 150°C, the materials were found to contain ~ 2 at.% hydrogen and 1–2 at.% oxygen by proton nuclear magnetic resonance (NMR) and energy dispersive X-ray analysis (EDX). The purified SWNTs from the same batch were divided into several groups and were processed by impact ball-milling in air for up to 20 min.

The processed nanotube materials were cast on flat 1 cm diameter stainless steel metal plates and were heated at 150°C under 10^{-6} Torr dynamic vacuum for a few hours after deposition. A Swagelok-type cell [16] was used with Li foil and the nanotube film as the two working electrodes. A polypropylene filter soaked with liquid electrolyte (1 M solution of $LiClO_4$ in 1:1 volume ratio of ethylene carbonate and dimethyl carbonate) was placed between the anode and cathode. The cell was discharged (intercalation) and charged (de-intercalation) under galvanostatic mode at 50 mA/g current (unless otherwise stated) between 0–3 V. The specific Li capacities (amount of Li intercalated per unit of carbon) were calculated from the time and the current used.

The charge-discharge data of purified SWNTs before processing are shown in Fig. 1. As reported previously [13], a composition of $Li_{5.4}C_6$ was obtained after the first discharge (intercalation). The amount of Li that can be removed from the nanotube electrode in the first charge, the reversible capacity C_{rev}, is $Li_{1.6}C_6$. The undesirably large irreversible capacity C_{irr} (Li_4C_6) is attributed to the large surface area of the SWNT electrode (estimated to be ~ 300 m^2/g by a N_2 BET measurement). Several samples were measured under the same conditions and showed reversible capacities in the range of Li_xC_6 ($x = 1.5$–1.7). A large voltage hysteresis between discharge and charge cycle was observed in all the samples measured.

Ball-milled samples showed enhanced performance. C_{rev} increased with increasing processing time, from $Li_{1.6}C_6$ for as-purified materials to Li_2C_6

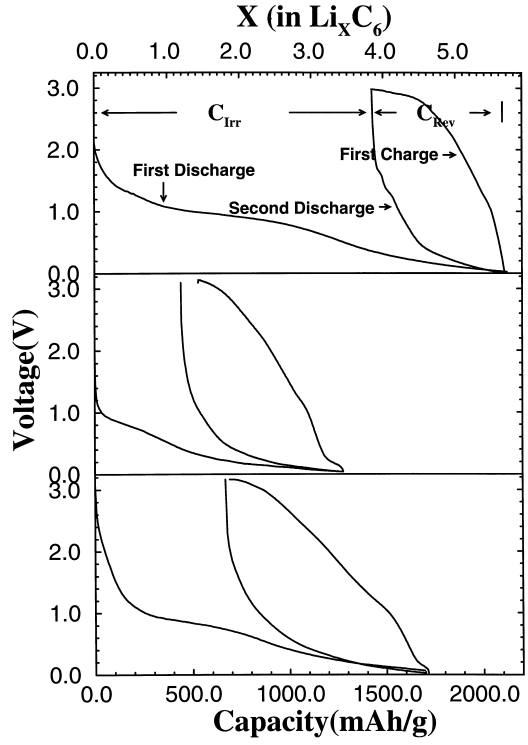

Fig. 1. Potential versus specific Li capacity data obtained from the purified (top), 1-min (middle) and 10-min (bottom) ball-milled SWNT samples. The data were collected at a constant current (50 mA/g). The purified and 10-min ball-milled SWNTs were deposited on Cu disks. The sample ball-milled for 1 min was deposited on stainless steel plate.

and $Li_{2.7}C_6$ after 1 and 10 min of processing, respectively (Fig. 1). Further processing led to a downturn of C_{rev}, to under $Li_{1.9}C_6$ in samples processed for 20 min. C_{irr} decreased from $Li_{3.2}C_6$ to $\sim Li_{1.4}C_6$ after 1 min of ball-milling, and then stayed essentially constant. $Li_{2.7}C_6$ is the highest reversible composition which, to our best knowledge, is the highest value reported for carbon materials (Metastable Li-rich graphite compound LiC_2 has been synthesized under pressure [17], but it decomposes rapidly at ambient conditions). The charge-discharge behavior of the sample milled for 10 min was also investigated under higher rates. C_{rev} decreased from $Li_{2.7}C_6$ at 50 mA/g current to $Li_{1.6}C_6$ at 500 mA/g. Very

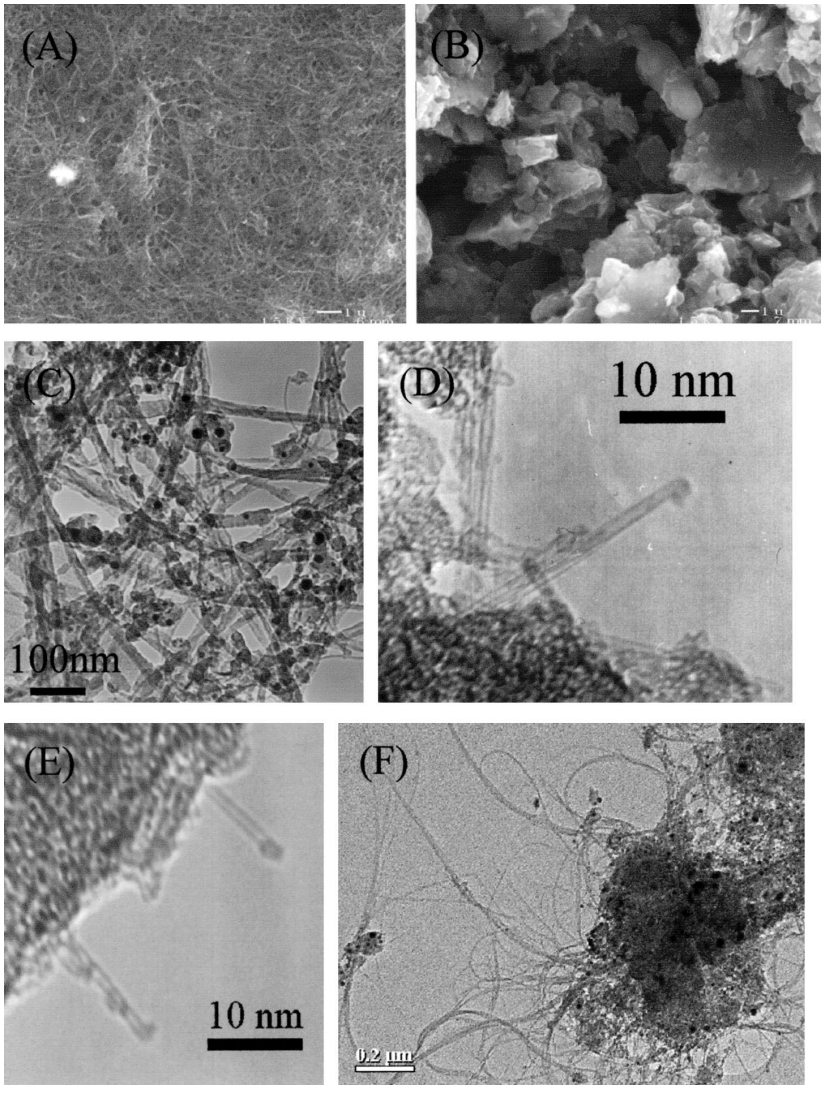

Fig. 2. SEM images of electrodes made of SWNTs before (A) and after (B) ball-milling. The lines in (A) are SWNT bundles. The images were taken using a JEOL 6300 microscope at 15 kV. TEM images of as-grown SWNTs (C) and SWNTs after 10 min of ball-milling are shown in (D)–(F). In contrast to the raw materials, densely packed particles were observed at low resolution. Isolated SWNTs and small SWNT bundles were found to protrude from the edges of these particles. These protruding nanotubes often show irregular structures at the ends. The TEM images were collected using a Phillips CM12 microscope operating at 100 kV.

little capacity decay ($< 1\%$) was observed after five charge–discharge cycles at 500 mA/g.

Fig. 2A,B show the SEM micrographs of electrodes made of purified SWNTs before and after ball-milling. A uniform and porous 'spaghetti'-type structure was observed before processing where the individual bundles (the lines in the SEM micrograph) were clearly resolved. Ball-milled SWNTs showed a different morphology. The surface is covered with 1–10 μm densely-packed particles (Fig. 2B). The increase in materials packing density is believed to be the reason for the reduction in C_{irr} observed in the ball-milled samples. The irreversible capacity is known to be associated with electrolyte decomposition and the formation of solid-electrolyte-interface (SEI) [18]). Fig. 2C–F show TEM micrographs of as-grown SWNTs and those taken from materials ball-milled for 10 min. In contrast to the as-grown materials where entangled SWNT bundles are resolved (Fig. 2C), only densely-packed particles were observed in the ball-milled materials at low resolution. Close examination along the edges of these particles showed individual nanotubes and small SWNT bundles (Fig. 2D,E). Observation of many nanotube ends suggests that the SWNTs were fractured and shortened by ball-milling (the ends are rarely observed in the as-grown and purified materials). Although irregular structures were often seen at the nanotube ends, the current TEM data can not resolve whether the ends remain opened. Further experiment showed the densely-packed particles were composed of mostly SWNTs that can be separated by sonication in dimethyl formamide (DMF), as illustrated by the TEM micrograph shown in Fig. 2F.

Raman spectra of the SWNTs before and after ball-milling were collected at room temperature using 514 nm laser light. Raman-active vibration modes associated with SWNTs and disordered carbon were observed in all the samples. The percentage of the SWNTs, estimated by the ratio between the total integrated intensities of the SWNT A_{1g}, E_{1g}, and E_{2g} modes around 1600 cm^{-1} and the mode associated with disordered carbon at ~ 1340 cm^{-1}, decreased only slightly with increasing ball-milling time up to 10 min (Fig. 3). This indicates that the majority phase in the sample ball-milled for 10 min is still the SWNTs. Further processing resulted in a significant increase in the intensity of the disordered carbon

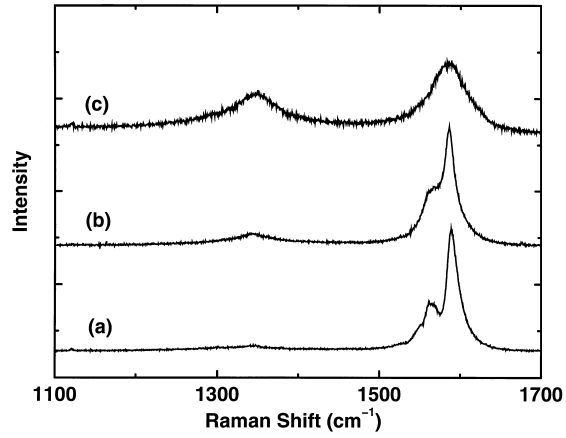

Fig. 3. Raman spectra of purified (a) and 10-min (b) and 20-min (c) ball-milled SWNT materials. The data were collected using 514 nm laser light and a micro-Raman spectrometer with a CCD detector at room temperature.

mode and broadening of the SWNT peaks, suggesting that SWNTs were converted to disordered/amorphous carbon. The Raman results support the electrochemical data where the highest C_{rev} of $Li_{2.7}C_6$ was obtained in samples processed for 10 min. The reduction of C_{rev} with further processing is attributed to the increase of the amorphous/disordered carbon content at the expense of the SWNTs.

Powder X-ray diffraction measurements indicate that ball-milling introduces disorder within the SWNT bundles. The diffraction patterns of the SWNTs before and after ball-milling are shown in Fig. 4. Significant changes in the relative intensities of the Bragg peaks originated from the SWNT bundles were observed. The diffraction patterns were simulated based on a 2D triangular lattice of SWNTs [7,1]. [2] The simulated patterns are plotted in Fig. 4B.

[2] When the SWNT bundle is composed of a mixture of different diameter nanotubes randomly occupying the lattice points, the unit cell structure factor can be approximated as:

$$S(Q) = \sum_{j=1}^{n} \left[\sum_{h=1}^{m} P_h F_{\mathrm{SWNT}}^{h}(QR_h) \right] \exp(-i\mathbf{Q}\cdot\mathbf{r}_j) \quad (1)$$

$$F_{\mathrm{SWNT}}^{h} = N_c^h f_c J_o(QR_h) \quad (2)$$

where R_h is the radius of the hth nanotube, $J_o(QR_h)$ the zero-order cylindrical Bessel function, N_c^h the total number of carbon atoms per hth tube per cell, f_c the atomic form factor of carbon, $\mathbf{r}_j$ the position of the jth lattice point, and P_h the occupancy of a SWNT with the radius R_h at the $\mathbf{r}_j$ position ($\sum_{h=1}^{m} P_h = 1$)

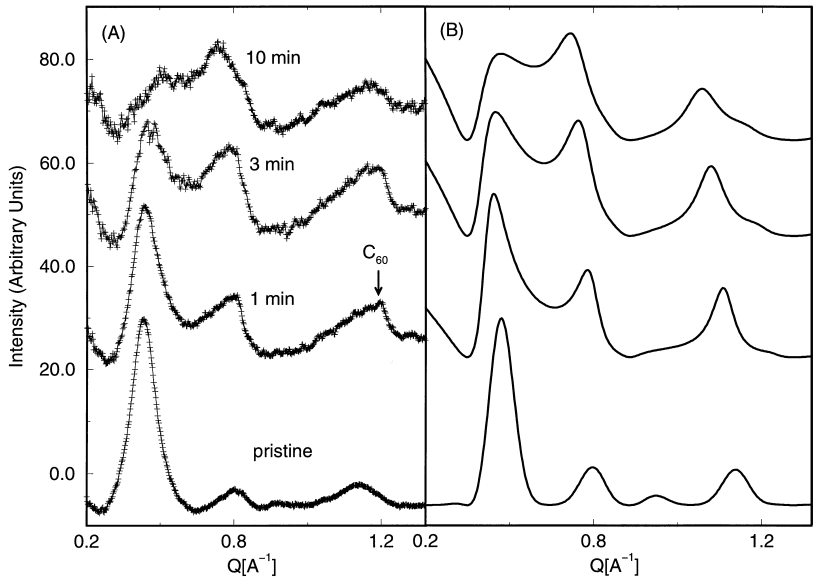

Fig. 4. (A): Powder X-ray diffraction patterns of raw and ball-milled SWNT samples after background subtraction. The data were collected using Cu K_α radiation and a 2D imaging plate detector. The exposure time was 2 h per spectrum. The spectrum from 1-, 3-, and 10-min ball-milled sample was multiplied by a factor of 2, 4 and 4, respectively. Arrows mark where diffraction intensities from C_{60} impurities are expected. (B): Simulated X-ray patterns. Simulation was carried out using a 2D triangular lattice with 50:50 mixture of two types of SWNTs with respective radius of 6.8 and 6.1 Å. A zero-order cylindrical Bessel function was used to approximate the scattering form factor of the nanotubes. The bundle size and the lattice parameters were varied until a reasonable agreement with the experimental spectrum was obtained.

The spectrum of the raw SWNTs can be simulated by a 50:50 random mixture of SWNTs with the respective radius of 6.8 and 6.1 Å, a lattice constant (a) of 16.2 Å and a Gaussian full-width-at-half-maximum (FWHM) of 0.06 Å^{-1}. The spectra of the ball-milled materials were simulated using the same structure model by adjusting the bundle diameter and the spacing between the individual SWNTs till a reasonable match with the experimental spectrum was obtained. A Lorentzian rather than a Gaussian function was needed to describe the Bragg peak line profile. For the sample that was ball-milled for 10 min, the X-ray diffraction pattern can be reasonably reproduced using $a = 18$ Å and a Lorentzian FWHM of 0.12 Å^{-1}. Due to modulation of the diffraction intensities by the scattering form factor of the nanotubes ($J_o(QR)$) [7,1], the apparent (10) peak position did not change much despite the 1.8 Å increase in the lattice constant. The increase of inter-SWNT spacing ($\Delta a = 1.8$ Å) and reduction in the bundle radial coherence length both indicate disorder within the bundle, consistent with the TEM results. Fig. 5 shows the changes of the lattice parameters and the FWHM of the SWNT (10) peak (obtained from the simulation) versus the ball-milling time. A corresponding broadening of the graphite/nanoparticle-(002) peak width was also observed. The interlayer/inter-shell spacing of the graphitic impurities increased from 3.37 to 3.44 Å after 10 min of processing, similar to the trend observed in ball-milled graphite [19].

The exact mechanism for the enhanced Li capacity in ball-milled SWNTs is not clear. Several models have been proposed to account for the excess Li capacity (beyond LiC_6) observed in carbonaceous materials, including formation of lithium multi-layers on graphene sheets [20], Li_2 covalent molecules [21], Li–C–H bonds [22–24] in soft carbons, filling of micro-cavities [25] and adsorption of Li on both sides of isolated graphene layers [23]. Disma et al. [19] showed that prolonged ball-milling induces disorder along the graphite c-axis and fractures the graphene layers. C_{rev} up to $Li_{1.9}C_6$ was observed after 80 h of milling. The large reversible capacity

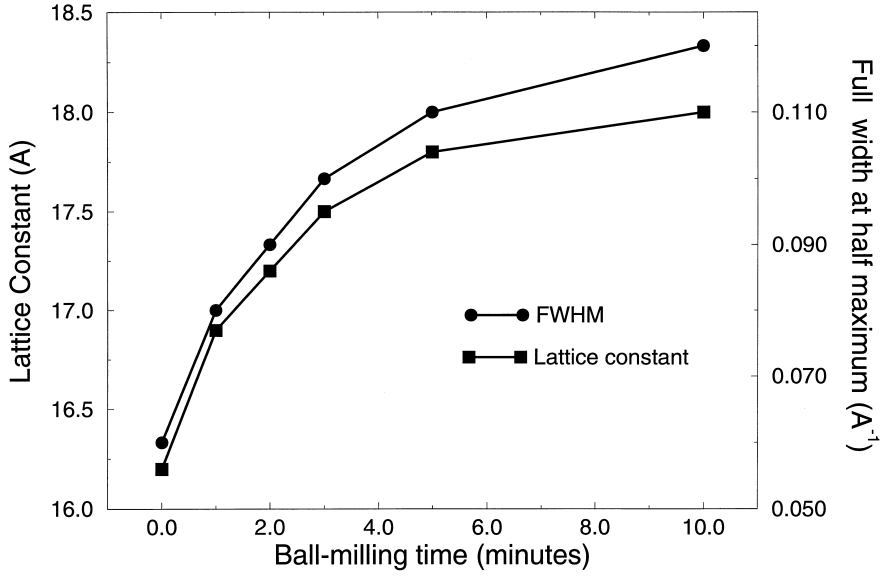

Fig. 5. The lattice parameters and Lorentzian FWHM of the (10) Bragg peak of the SWNT 2D triangular lattice obtained from simulation are plotted versus the ball-milling time.

was attributed to adsorption of Li ions on both sides of isolated graphene layers [19]. Xing et al. reported that ball-milling increases C_{rev} of 'sugar-carbon' from $Li_{1.5}C_6$ to as high as Li_2C_6 [26]. It was proposed that in ball-milled sugar-carbons, the excess reversible capacity rises from lithium reaction with carbon radicals at the edges of the fractured graphene sheets and with H- and O-containing surface functional groups [26]. Similar to the data for the ball-milled SWNTs obtained in this experiment, both the ball-milled graphite and sugar-carbon show a large voltage hysteresis between charge and discharge.

Single-walled nanotubes are relatively defect free [7] (compared to disordered carbon and MWNTs) and are unlikely to have meaningful amounts of functional groups on the side-walls without processing. After ball-milling, it is possible that the fractured nanotubes are terminated chemically. Considering the aspect ratio of the nanotubes, the contribution of the ends should be small. Proton nuclear magnetic resonance measurements showed that the raw and ball-milled SWNTs used in this study contain ~ 2 at.% proton after annealing at 150°C in vacuum. Similarly, the oxygen concentration remained at ~ 2 at.% level after ball-milling, indicating that H- and O-containing functional groups do not play important roles in Li storage in SWNTs. The changes in the structure and morphology observed in the ball-milled SWNTs suggest the enhanced capacity is related to the degree of disorder within the bundle, and lithium diffusion into the inner cores of the fractured nanotubes. The large voltage hysteresis between charge and discharge is at least partially related to the kinetics of lithium diffusion into the inner cores of the SWNTs. Preliminary experiments have shown that the hysteresis can be reduced by cutting the nanotubes to shorter segments.

Acknowledgements

We acknowledge support from the Office of Naval Research (through a MURI program N00014-98-1-0597) and the Petroleum Research Fund. C.B. is supported by a NASA graduate fellowship.

References

[1] W. Andreoni (Ed.), The Physics of Fullerene Based and Fullerene-Related Materials, Kluwer, Dordrecht, 2000.

[2] G. Pistoria (Ed.), Lithium Batteries: New Materials, Developments and Perspectives, Elsevier, Amsterdam, 1994.
[3] J. Fischer, in: A.P. Legrand, S. Flandrois (Eds.), Chemical Physics of Intercalation Compounds, vol. 59, Plenum, New York, 1987.
[4] S. Iijima, Nature 354 (1991) 56.
[5] O. Zhou et al., Science 263 (1994) 1744.
[6] S. Suzuki, M. Tomita, J. Appl. Phys. 79 (1996) 3739.
[7] A. Thess et al., Science 273 (1996) 483.
[8] R. Lee et al., Nature 388 (1997) 255.
[9] C. Bower, S. Suzuki, K. Tanigaki, O. Zhou, Appl. Phys. A 67 (1998) 47.
[10] A. Rao et al., Nature 388 (1997) 257.
[11] S. Suzuki, C. Bower, O. Zhou, Chem. Phys. Lett. 285 (1998) 230.
[12] A. Claye, R. Lee, Z. Benes, J. Fischer, J. Electrochem. Soc. 406 (2000) in press.
[13] B. Gao, A. Kleinhammes, X.P. Tang, C. Bower, L. Fleming, Y. Wu, O. Zhou, Chem. Phys. Lett. 307 (1999) 153.
[14] E. Frackowiak et al., Carbon 37 (1999) 61.
[15] K. Shelimov et al., Chem. Phys. Lett. 282 (1998) 429.
[16] D. Guyomard, J. Tarascon, J. Electrochem. Soc. 139 (1992) 937.
[17] V. Avdeev, V. Nalimova, K. Semenenko, High Pressure Res. 6 (1990) 11.
[18] M. Winter, J. Besenhard, K. Spahr, P. Novak, Adv. Mater. 10 (1998) 725.
[19] F. Disma, L. Aymard, L. Dupont, J. Tarascon, J. Electrochem. Soc. 143 (1996) 3959.
[20] R. Yazami, M. Munshi, in: M. Munshi (Ed.), Handbook of Solid State Batteries and Capacitors, World Scientific, Singapore, 1995, p. 425.
[21] K. Sato et al., Science 264 (1994) 556.
[22] T. Enoki, S. Miyajima, M. Sano, H. Inokuchi, J. Mater. Res. 5 (1990) 435.
[23] J. Dahn, T. Zhang, Y. Liu, J. Xue, Science 270 (1995) 590.
[24] P. Zhou, P. Papanek, R. Lee, J. Fischer, J. Electrochem. Soc. 144 (1997) 1744.
[25] H. Fujimoto, A. Mabuchi, K. Tokumitsu, T. Kasuh, J. Power Sources 54 (1995) 440.
[26] W. Xing, R. Dunlap, J. Dahn, J. Electrochem. Soc. 145 (1998) 62.